forces along the snake body to maintain propulsion, was implemented on a physical snake robot placed in a course with different obstacle configurations. The experiments showed that the proposed controller successfully maintained the overall forward propulsion of the robot in all the considered obstacle courses, which supports the underlying control principle of rotating contacted links in order to increase the propulsive force on the snake robot.

The experimental results have inspired the authors to, in future work, pursue the development of continuous controllers for obstacle-aided locomotion, where jam resolution is a continuous action that is performed in parallel with the cyclic wave motion of the snake robot.

REFERENCES

[1] J. Gray, "The mechanism of locomotion in snakes," *J. Exp. Biol.*, vol. 23, no. 2, pp. 101–120, 1946.

[2] B. Moon and C. Gans, "Kinematics, muscular activity and propulsion in gopher snakes," *J. Exp. Biol.*, vol. 201, pp. 2669–2684, 1998.

[3] A. A. Transeth, R. I. Leine, C. Glocker, K. Y. Pettersen, and P. Liljebäck, "Snake robot obstacle aided locomotion: Modeling, simulations, and experiments," *IEEE Trans. Robot.*, vol. 24, no. 1, pp. 88–104, Feb. 2008.

[4] J. Ostrowski and J. Burdick, "Gait kinematics for a serpentine robot," in *Proc. IEEE Int. Conf. Robot. Autom.*, Apr. 1996, vol. 2, pp. 1294–1299.

[5] K. J. Dowling, "Limbless locomotion. learning to crawl with a snake robot" Ph.D. dissertation, Robot. Inst., Carnegie Mellon Univ., Pittsburgh, PA, Dec. 1997.

[6] S. Ma, "Analysis of creeping locomotion of a snake-like robot," *Adv. Robot.*, vol. 15, no. 2, pp. 205–224, 2001.

[7] M. Saito, M. Fukaya, and T. Iwasaki, "Serpentine locomotion with robotic snakes," *IEEE Contr. Syst. Mag.*, vol. 22, no. 1, pp. 64–81, Feb. 2002.

[8] C. Ye, S. Ma, B. Li, and Y. Wang, "Turning and side motion of snake-like robot," in *Proc. IEEE Int. Conf. Robot. Autom.*, 2004, vol. 5, pp. 5075–5080.

[9] F. Chernousko, "Modelling of snake-like locomotion," *Appl. Math. Comput.*, vol. 164, no. 2, pp. 415–434, May 2005.

[10] J. Gonzalez-Gomez, H. Zhang, and E. Boemo, *Locomotion Principles of 1D Topology Pitch and Pitch-Yaw-Connecting Modular Robots*. Vienna, Austria: Advanced Robotics Systems International and I-Tech Education, Sep. 2007, ch. 24, pp. 403–428.

[11] S. Hirose, *Biologically Inspired Robots: Snake-Like Locomotors and Manipulators*. Oxford, U.K.: Oxford Univ. Press, 1993.

[12] Z. Bayraktaroglu and P. Blazevic, "Understanding snakelike locomotion through a novel push-point approach," *J. Dyn. Syst.—Trans. ASME*, vol. 127, no. 1, pp. 146–152, Mar. 2005.

[13] Z. Y. Bayraktaroglu, "Snake-like locomotion: Experimentations with a biologically inspired wheel-less snake robot," *Mech. Mach. Theory*, vol. 44, no. 3, pp. 591–602, 2008.

[14] Y. Shan and Y. Koren, "Design and motion planning of a mechanical snake," *IEEE Trans. Syst. Man, Cybern.*, vol. 23, no. 4, pp. 1091–1100, Jul./Aug. 1993.

[15] H. Date and Y. Takita, "Adaptive locomotion of a snake like robot based on curvature derivatives," in *Proc. IEEE/RSJ Int. Conf. Intell. Robots Syst.*, San Diego, CA, Oct./Nov. 2007, pp. 3554–3559.

[16] A. M. Andruska and K. S. Peterson, "Control of a snake-like robot in an elastically deformable channel," *IEEE/ASME Trans. Mechatron.*, vol. 13, no. 2, pp. 219–227, Apr. 2008.

[17] A. Kuwada, S. Wakimoto, K. Suzumori, and Y. Adomi, "Automatic pipe negotiation control for snake-like robot," in *Proc. IEEE/ASME Int. Conf. Adv. Intell. Mechatron.*, Jul. 2008, pp. 558–563.

[18] P. Liljebäck, K. Y. Pettersen, Ø. Stavdahl, and J. T. Gravdahl, "Hybrid modelling and control of obstacle-aided snake robot locomotion," *IEEE Trans. Robot.*, vol. 26, no. 5, pp. 781–799, Oct. 2010.

[19] R. Goebel, R. Sanfelice, and A. Teel, "Hybrid dynamical systems," *IEEE Contr. Syst. Mag.*, vol. 29, no. 2, pp. 28–93, 2009.

[20] P. Liljebäck, K. Y. Pettersen, and Ø. Stavdahl, "A snake robot with a contact force measurement system for obstacle-aided locomotion," in *Proc. IEEE Int. Conf. Robot. Autom.*, Anchorage, AK, 2010, pp. 683–690.

[21] T. Lochmatter, P. Roduit, C. Cianci, N. Correll, J. Jacot, and A. Martinoli, "Swistrack—A flexible open source tracking software for multi-agent systems," in *Proc. IEEE/RSJ Int. Conf. Intell. Robots Syst.*, 2008, pp. 4004–4010.

Minimum-Time Trajectory for Three-Wheeled Omnidirectional Mobile Robots Following a Bounded-Curvature Path With a Referenced Heading Profile

Ki Bum Kim and Byung Kook Kim

***Abstract*—The minimum-time trajectory planning problem for three-wheeled omnidirectional mobile robots (TOMRs) is solved based on the combined dynamic model of a mobile robot and dc motor actuators, under the constraint of bounded control inputs due to the battery voltage. We constrain that the bounded-curvature path based on a smooth road (which is described as a clothoid) be given for the translational motion of the TOMR and that the reference profile with respect to the path-length parameter be predetermined for the heading motion of the TOMR. The dynamics of the TOMR is transformed into normal and tangent spaces for motion analysis on the bounded-curvature path. We find out the time-optimality condition of the TOMR, which imposes that the input voltage vector of three motors should have at least one extreme component. Based on the optimality condition, we present a systematic way to construct the optimal control input vector. Finally, several examples are analyzed by the use of the proposed method.**

***Index Terms*—Bounded-curvature path, dynamics, minimum-time trajectory, three-wheeled omnidirectional robot.**

I. INTRODUCTION

Mobile robots have been used in various applications to increase efficiency or to replace human labor. Mobile robots can be divided into two types based on their motion generation capabilities: nonholonomic and holonomic mobile robots. In contrast with nonholonomic mobile robots, such as those with two-wheeled differential drive, omnidirectional mobile robots with more than three wheels are holonomic, and their translational and rotational motions can be controlled independently at any time [1]. In other words, omnidirectional mobile robots can move sideways and forward in addition to rotating. For example, when a mobile robot moves along a given path, as shown in Fig. 1(a), a two-wheeled differential mobile robot must stop at the end of the first straight line, rotate in place, and move along the second straight line. However, the rotation in place can be an unnecessary step for a three-wheeled omnidirectional mobile robot (TOMR) because TOMRs can perform the translational and rotational motions simultaneously on the first straight line. As another example, a two-wheeled differential mobile robot could never follow the path that is shown in Fig. 1(b), whereas a TOMR with rotation can traverse the arc path. Because of their high mobility, omnidirectional mobile robots have been widely used for many missions in complex environments. Omnidirectional mobile robots have been studied for use in robot-soccer games, home security, cleaning, rehabilitation, and so on [2]–[7].

In general, the trajectory planning problem for mobile robots is to find the desired trajectory with respect to a given objective function.

Manuscript received August 14, 2010; revised February 15, 2011; accepted March 29, 2011. Date of publication May 10, 2011; date of current version August 10, 2011. This paper was recommended for publication by Associate Editor K. Iagnemma and Editor G. Oriolo upon evaluation of the reviewers' comments. This work was supported in part by the Ministry of Knowledge Economy under the Human Resources Development Program for Convergence Robot Specialists.

The authors are with the Department of Electrical Engineering, Korea Advanced Institute of Science and Technology, Daejeon 305-701, Korea (e-mail: kbkim@rtcl.kaist.ac.kr; bkkim@ee.kaist.ac.kr).

Color versions of one or more of the figures in this paper are available online at http://ieeexplore.ieee.org.

Digital Object Identifier 10.1109/TRO.2011.2138490

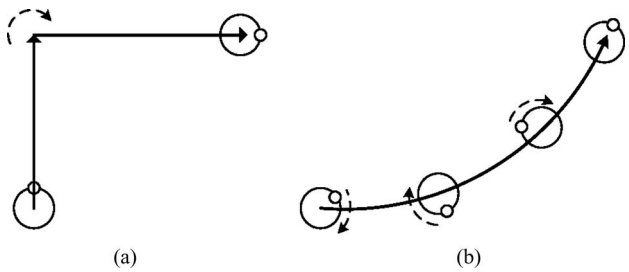

Fig. 1. Illustrative paths for the motion characteristics of omnidirectional mobile robots. The large circle represents the robot body, and the small circle represents the robot heading.

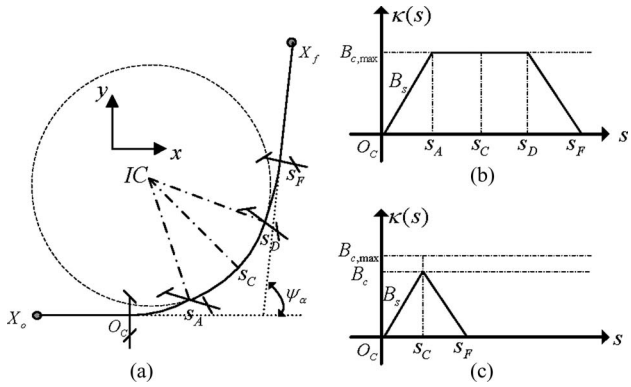

Fig. 2. Bounded-curvature path. (a) SAS path (straight line, arc by clothoid, and straight line) in the base coordinate frame. (b) Curvature graph with respect to path length; in this case, the curvature is saturated at its maximum bound. (c) Curvature graph with respect to path length for the case when the curvature is not saturated.

In this paper, we focus on the minimization of the arrival time to the final state by the use of TOMR dynamics. However, because of the complexity of TOMR dynamics, it is difficult to directly analyze the time optimality of a TOMR with boundary conditions on a free path. Thus, our study is restricted to a specified path.

A specified path can be considered as the outcome of high-level path planning based on a mission for a mobile robot. Path planning often provides a combination of simple paths: straight lines and circular arcs (with a step change in the angular velocity between the straight line and the arc segment). In light of the dynamics of the platform, we replace the circular arc with a bounded-curvature clothoid path. The clothoid guarantees that the robot can exactly follow the path curve with continuous velocity, which results in smooth motion.

Much research has been done on the mechanical design of omnidirectional mobile robot. For a four-wheeled omnidirectional mobile robot, the dynamic model was established in [8], and a control redundancy was addressed in [9]. In particular, we focus on the dynamics of a TOMR with orthogonal wheels as described in [10] and [11], where the coupling terms of the linear and angular velocities are considered to build a more accurate description of the dynamics.

In related works on the time optimality of mobile robots, many researchers have studied the time-optimal problem for two-wheeled differential drive mobile robots [12]–[19]. Recently, a few researchers have made outstanding contributions to the minimum-time study of TOMRs. Near time-optimal analysis, as described in Kalmar-Nagy *et al.* [20], aims to decrease the computational time for adoption in real-time applications, but it does not fully consider the voltage bounds and the TOMR dynamics in its optimality analysis. Fu *et al.* [21] computed the time-optimal trajectory of a TOMR with a heuristic algorithm that combined a genetic algorithm and nonlinear programming. However, the result in that paper did not offer general characteristics for the time-optimal motion of a TOMR. Balkcom *et al.* [22] proposed a classification for time-optimal trajectories based on spin-in-place, circular-arc, and singular translation as the basic optimal motions, and they made steps toward an analytical time-optimal study of a TOMR over a free path. However, their research was based on kinematics and did not specify which trajectory would be optimal for a specific configuration. In a previous work [11], [23], we studied the time-optimal straight-line trajectory for a TOMR. However, that work focused only on straight-line paths.

In this paper, we deal with the time-optimal trajectory of a TOMR with battery-voltage constraints and a bounded-curvature path constraint with a referenced heading profile.

First, we consider a *symmetric bounded-curvature path*, which closely resembles a smooth highway exit. A symmetric bounded-curvature path is composed of three parts: a straight line, a clothoid arc with bounded curvature, and another straight line (SAS). For simplicity, we let the maximum curvature and the slope of curvature be given. Indeed, it is not necessary that a bounded-curvature path by the use of a clothoid be symmetric. However, this constraint is reasonable if the robot is required to traverse the path in the reverse direction. Moreover, since a clothoid arc with zero curvature is regarded as a straight line, we can say that the SAS path in this paper also includes the straight-line path.

We also constrain that a reference heading profile be given. In other words, we let the high-level path planner provide the heading information for all positions in the planar path. Although this constraint makes the scope of our study narrow, we can say that the necessity of a constrained heading depends entirely on the mission of the robot. For example, when a TOMR with a fixed inlet is used to clean a room, a heading constraint is required so that the robot can clean the room evenly.

Finally, for the time-optimality analysis, we consider the bound of control inputs to motors rather than acceleration or torque limits. Since electric dc motors are widely used as wheel actuators and battery voltages are used as the final input to the motors (e.g., by the use of a pulsewidth modulation signal), it is practical to consider the constraint on the battery-voltage bound in real applications [12].

The remainder of this paper is organized as follows. In Section II, SAS paths with bounded curvature and the modified TOMR dynamics for parameterized paths are described. In Section III, we define our problem, investigate the optimality condition for the battery-voltage inputs, and discuss the construction of the optimal input vector. Simulation results with three referenced heading profiles and concluding remarks are shown in Sections IV and V.

II. Path and Dynamics

In this section, we introduce the representation of an SAS path as the curvature function with respect to the path-length parameter and how to describe the TOMR dynamics with bounded voltage input at any point of the SAS path. Additionally, we determine the input condition to prevent TOMR from deviating from the SAS path.

A. Straight–Arc–Straight Path With Bounded Curvature

We consider a symmetric bounded-curvature path in SAS form, as shown in Fig. 2(a). The symbols used in Fig. 2 are listed in Table I. Similar to a conventional smooth road, the path orientation is required to change by an amount ψ_α through a symmetric clothoid path with

TABLE I
PARAMETERS OF THE SAS PATH

Parameter	Description
$\psi(s)$	Path orientation with respect to path-length parameter
ψ_α	Amount of path orientation changed by clothoid arc
ψ_l	Smallest path orientation for trapezoidal curvature function
$\kappa(s)$	Curvature function with respect to path-length parameter
B_s, B_c	Slope of curvature, bounded curvature in clothoid arc
$B_{c,\max}$	Maximum bounded curvature
X_0, X_f	Starting, ending points of SAS path
O_C, s_A	Starting, ending points of angular acceleration in clothoid
s_D, s_F	Starting, ending points of angular deceleration in clothoid
s_C	Center point of clothoid

a bounded curvature. Two straight lines are connected to the clothoid path at both sides. In other words, a symmetric bounded-curvature path is composed of two straight lines and a clothoid arc (SAS path). Conventionally, we let the slope of curvature be given as B_s during acceleration and deceleration. A clothoid arc with a bounded curvature $B_c (\leq B_{c,\max})$ can be represented as a trapezoidal curvature $\kappa(s)$ with respect to the path length, as shown in Fig. 2(b).

From the definition of a clothoid, we can represent major points on the clothoid path as follows:

$$s_A = \frac{B_c}{B_s}, \quad s_D = \frac{\psi_\alpha}{B_c}, \quad s_F = \frac{\psi_\alpha}{B_c} + \frac{B_c}{B_s}. \tag{1}$$

Using the relation $\psi(s) = \int_s \kappa(s) ds$ and (1), we can calculate the path angle at s_A and s_D as follows:

$$\psi(s_A) = \frac{B_c^2}{2B_s}, \quad \psi(s_D) = \psi_\alpha - \frac{B_c^2}{2B_s}. \tag{2}$$

In addition, for smaller orientation changes ($\psi_\alpha < \psi_l$), the curvature of the clothoid becomes a triangular form as shown in Fig. 2(c). In this case, s_A and s_D become the same point.

Since the area of the curvature graph is equal to ψ_α, we can obtain the equation for B_c from (1) and (2) as follows:

$$B_c = \begin{cases} \sqrt{\psi_\alpha B_s}, & \text{for } \psi_\alpha \leq \psi_l \\ B_{c,\max} (= \sqrt{\psi_l B_s}), & \text{for } \psi_\alpha > \psi_l. \end{cases} \tag{3}$$

Therefore, with given B_s and $B_{c,\max}$, we can construct the curvature function $\kappa(s)$ for a bounded clothoid path.

For the path constraint on the TOMR motion, we consider a symmetric bounded-curvature path as represented in this section. In particular, an SAS path with $\psi_\alpha = 0$ can be regarded as a straight-line path. Our studies are not focused on the results of high-level path planning. Instead, we discuss the general properties of time-optimal motion of TOMR following a curved path.

B. Dynamics of the Three-Wheeled Omnidirectional Mobile Robot

The TOMR that is considered in this paper consists of a robot body and three sets of omnidirectional wheel assemblies equally spaced at 120° from one another. In other words, each wheel can roll perpendicular to the wheel axis while freewheeling in the other direction. A TOMR is schematically depicted in Fig. 3, where m is the total mass of the robot, J is the total inertia of robot rotation, r is the radius of each wheel, l is the distance between the center of the robot and one wheel, and f_i is the force acting in the tangential direction on each wheel. $\mathbf{x} = [x, y, \phi]^T$ represents the robot position in the base coordinate frame, and $\mathbf{x_m} = [x_m, y_m, \phi]^T$ represents the robot position in the robot coordinate frame. The x_m-axis is perpendicular to the rotational direction of the first wheel.

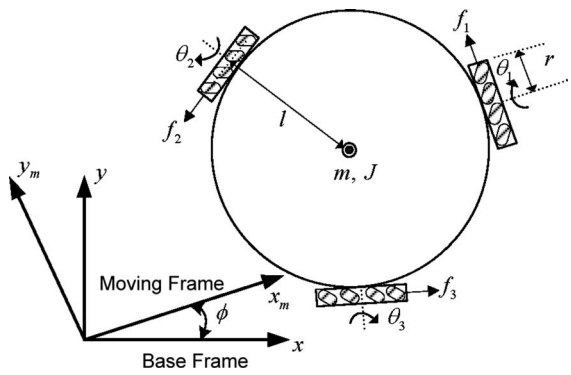

Fig. 3. Schematic drawing of a TOMR.

In this paper, we use the TOMR dynamics including the mobile robot and motor actuators suggested in [11], where the control input to the motors $\mathbf{u} = [u_1, u_2, u_3]^T$ is normalized by the battery voltage. Here, we assume that the robot mass is uniformly distributed about its center and each wheel is characterized by the orthogonal wheel concept [1]. We also assume that the electrical time constant of the wheel motor is far smaller than the mechanical time constant and can be neglected, and we assume that the friction force can be represented by a viscous coefficient constant.

The dynamic equations in the base coordinate frame are represented as follows:

$$\ddot{x} = -a\dot{x} - \dot{\phi}\dot{y} + ahu_x \tag{4}$$

$$\ddot{y} = -a\dot{y} + \dot{\phi}\dot{x} + ahu_y \tag{5}$$

$$\ddot{\phi} = -b\dot{\phi} + bh(2l)^{-1}u_\phi. \tag{6}$$

Here, a and b are the approximate decay constants of the linear and angular TOMR velocities, respectively. The constant h depends on the floor, motor specification, supply voltage, and wheel radius. The coordinated inputs to the dynamic equations $[u_x, u_y, u_\phi]^T$ are represented as

$$u_x = -\sin(\phi)u_1 - \sin(\phi + 2\pi/3)u_2 - \sin(\phi - 2\pi/3)u_3 \tag{7}$$

$$u_y = \cos(\phi)u_1 + \cos(\phi + 2\pi/3)u_2 + \cos(\phi - 2\pi/3)u_3 \tag{8}$$

$$u_\phi = u_1 + u_2 + u_3. \tag{9}$$

Equations (4)–(6) describe the way TOMR motion is generated from the battery voltage as the motor control input.

In the time-optimal straight-line problem with self-rotation in [23], we know that an additional compensation force is required to prevent the TOMR to deviate from the straight-line path. Therefore, it is necessary to investigate whether a similar compensation force is required for the time-optimal trajectory of a TOMR following a bounded-curvature path. To aid in this investigation, we transform the TOMR dynamics into a new coordinate system, as shown in Fig. 4. Let ψ be the path orientation at any point along the curved path. The coupling terms in (4) and (5) stem from the velocity relationship between the local robot coordinate frame and the base coordinate frame:

$$\dot{\mathbf{x}} = \mathbf{R}(\phi)\dot{\mathbf{x}}_\mathbf{m} \tag{10}$$

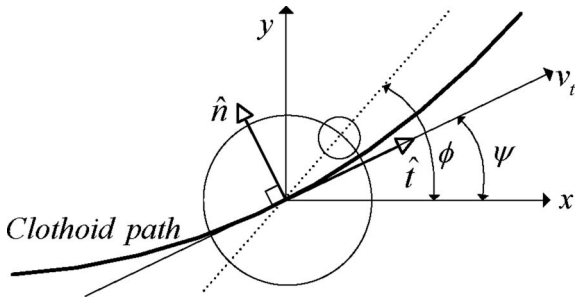

Fig. 4. Transformed coordinate at an arbitrary point along the clothoid path.

where

$$\mathbf{R}(\phi) = \begin{bmatrix} \cos\phi & -\sin\phi & 0 \\ \sin\phi & \cos\phi & 0 \\ 0 & 0 & 1 \end{bmatrix}.$$

If we denote the tangential and normal directions at any point in the clothoid path by $\hat{t}$ and $\hat{n}$, respectively, we can construct the velocity relationship in our new coordinate frame as follows:

$$\dot{\mathbf{x}}_\mathbf{t} = \mathbf{R}(\phi - \psi)\dot{\mathbf{x}}_\mathbf{m} \tag{11}$$

where $\mathbf{x_t} = [\hat{t}, \hat{n}, \phi]^T$. If we denote the velocities in the $\hat{t}$ and $\hat{n}$ directions by v_t and v_n, respectively, then we can represent the TOMR dynamics in a similar form to (4) and (5):

$$\dot{v}_t = -av_t - (\dot{\phi} - \dot{\psi})v_n + ahu_t \tag{12}$$

$$\dot{v}_n = -av_n + (\dot{\phi} - \dot{\psi})v_t + ahu_n. \tag{13}$$

Furthermore, we can represent the coordinated input in the transformed coordinate frame as

$$\begin{aligned} u_t = &-\sin(\phi - \psi)u_1 \\ &- \sin(\phi - \psi + 2\pi/3)u_2 - \sin(\phi - \psi - 2\pi/3)u_3 \end{aligned} \tag{14}$$

$$\begin{aligned} u_n = &\cos(\phi - \psi)u_1 \\ &+ \cos(\phi - \psi + 2\pi/3)u_2 + \cos(\phi - \psi - 2\pi/3)u_3. \end{aligned} \tag{15}$$

Thus, we use (12), (13), and (6) for TOMR dynamics in the transformed coordinate frame after Section III.

In fact, when the TOMR dynamics in the transformed coordinate frame is derived from (11), the time derivative of $\mathbf{R}(\phi - \psi)$ determines whether a compensation force in the normal direction is necessary. If $\phi - \psi$ is constant, we do not have to consider any coupling terms. Therefore, no compensation force is required for the TOMR to stay on the path. In other words, there is no additional compensation force in the normal direction for $\dot{v}_n = v_n = 0$. Otherwise, we should consider the additional compensation force in the normal direction for $\dot{v}_n = v_n = 0$ as follows:

$$u_n = -\frac{1}{ah}v_t(\dot{\phi} - \dot{\psi}). \tag{16}$$

In summary, when the rate of change of the TOMR heading and path orientation deviate, a compensation force is required to prevent path overshoot. This finding supports the observation that a heading change during the straight-line motion of a TOMR generates a Coriolis effect [23].

C. Control Input Bounds

In this paper, we deal with TOMR dynamics containing dc motor actuators with bounded control inputs, which is caused by the battery-voltage bound. Since each component of the input vector is normalized, we have an input constraint as follows:

$$|u_i| \leq 1, \qquad \text{for } i = 1, 2, 3. \tag{17}$$

III. Time-Optimal Analysis

In this section, based on the background in Section II, we define the main problem dealt with in this paper. Then, we find the time-optimality condition for the battery-voltage inputs. Finally, the construction of the optimal input vector is proposed in detail.

A. Problem Definition

Based on the TOMR dynamics, we are going to study the minimum-time trajectory for a TOMR following an SAS path with a referenced heading profile. We constrain that the SAS path characterized by the maximum curvature, the slope of curvature, and ψ_α be given, as shown in Fig. 2. We also constrain that the reference heading profile $G(s)$ with respect to the path length s be given as $G(s) = \int g(s)ds$. Here, $g(s)$ is the rate of heading change with respect to the path length. This constraint guarantees that the TOMR heading can follow the given reference heading profile, since $G(s)$ changes smoothly with respect to the path length.

Without loss of generality, we let the TOMR start at the origin in the base coordinate frame and move initially toward the positive *x*-direction in the base coordinate frame. Then, we can define *the minimum-time trajectory planning problem of a TOMR with a constrained heading and SAS path constraints (MTTP-C-SAS)* as follows.

Problem 1 (MTTP-C-SAS): Suppose that a TOMR moves in an SAS path with the curvature function $\kappa(s)$ and that the referenced profile for the TOMR heading is given as $G(s) = \int g(s)ds$. Find $\mathbf{u}$ according to

$$\begin{aligned} &\min\ t_f \text{ subject to} \\ &\quad \dot{\mathbf{x}} = \mathbf{f}(\mathbf{x}, \mathbf{u}) \\ &|u_i| \leq 1, \qquad \text{for } i = 1, 2, 3. \end{aligned}$$

Here, t_f is the final time; $\dot{\mathbf{x}} = \mathbf{f}(\mathbf{x}, \mathbf{u})$ is equivalent to (12), (13), and (6); and the boundary conditions are $\mathbf{x}(0) = [0, 0, \phi_0]^T$, $\mathbf{x}(t_f) = [x_f, y_f, \phi_f]^T$, and $\dot{\mathbf{x}}(0) = \dot{\mathbf{x}}(t_f) = [0, 0, 0]^T$.

B. Optimality Condition

From (12) and $v_n \equiv 0$, we can represent the TOMR dynamics for the translational motion in the transformed coordinate frame as follows:

$$\dot{v}_t = -av_t + ahu_t. \tag{18}$$

The translational direction of the TOMR is constrained by the linear velocity of the TOMR and the curvature of the SAS path, i.e., $\dot{\psi} = \kappa(s)v_t$.

In addition, from the problem statement of *MTTP-C-SAS*, the TOMR heading is constrained by the linear velocity of the TOMR and the rate of heading change, i.e., $\dot{\phi} = g(s)v_t$. In other words, the constraint of the TOMR heading with the referenced heading profile $G(s)$ provides another input constraint for u_ϕ (the input of $\dot{\phi}$ dynamics).

Hence, we should consider the input constraint for u_n to prevent a path overshoot. At the same time, we consider the input constraint for u_ϕ to meet a given reference heading profile. Then, we can obtain the time-optimality condition for *MTTP-C-SAS* as follows.

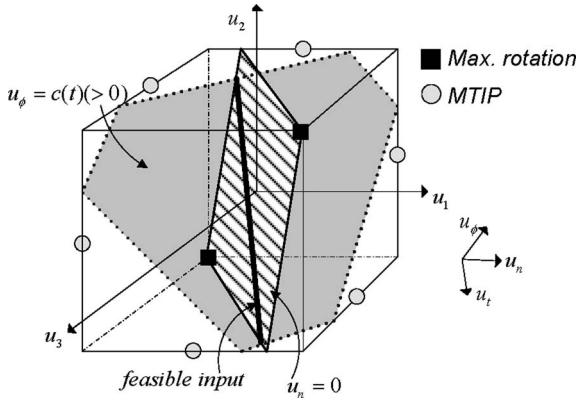

Fig. 5. Feasible input region of *MTTP-C-SAS* in the $\mathbf{u}$ cube. The plane of $u_n = 0$ is drawn when $\phi - \psi$ is any angle in the range $(-\pi/6, 0)$.

Theorem 1 (Optimality Condition): For the time optimality of TOMR in *MTTP-C-SAS*, the battery input vector of TOMR should have at least one extreme component.

Proof: Let the state vector be $\mathbf{z} = [s, v_t]^T$. Then, using the corresponding costate vector $\boldsymbol{\lambda} = [\alpha, \beta]^T$, we can construct the Hamiltonian for *MTTP-C-SAS* with (18) as follows:

$$H(\mathbf{z}, \boldsymbol{\lambda}, \mathbf{u}, \mathbf{t}) = \mathbf{1} + \boldsymbol{\lambda}^{\mathrm{T}} \dot{\mathbf{z}} = \mathbf{1} + (\alpha - a\beta) v_t + \beta a h u_t. \tag{19}$$

Although u_t of (14) depends on ϕ and ψ, u_t in (19) is obviously independent of the state vector $\mathbf{z} = [s, v_t]^T$. Thus, from $-\dot{\boldsymbol{\lambda}} = \partial H / \partial \mathbf{z}$, the costate functions are represented as

$$\alpha = \text{negative constant} \tag{20}$$

$$-\dot{\beta} = \alpha - a\beta. \tag{21}$$

Since the stationary condition of $\partial H / \partial \mathbf{u} = \mathbf{0}$ has no solution, we must directly investigate the given Hamiltonian.

As shown in Fig. 5, the objective is to find u_t that minimizes (19) with $u_n = -(1/(ah))v_t(\dot{\phi} - \dot{\psi})$ and $u_\phi = c(t)$ in the $\mathbf{u}$ cube. Here, the $\mathbf{u}$ cube is the input domain generated by (17) and the six maximum translational input points (*MTIP*s) are defined as the *two-extreme* input points in the straight-line movement of the TOMR without self-rotation in [11]. In addition, $c(t)$ is the rotational input magnitude of the TOMR so that the TOMR can meet the referenced heading at any point in the SAS path. Because of the orthogonality of the coordinated inputs ($u_t \perp u_n \perp u_\phi$), the feasible input region is a line in the $\mathbf{u}$ cube, and any optimal input vector is located on a face of the $\mathbf{u}$ cube. Hence, the optimality condition for *MTTP-C-SAS* is that the battery input vector should have at least one extreme component. ■

In fact, there are two input vectors located on a face of the $\mathbf{u}$ cube. Which input vector minimizes (19) depends on the sign of the costate function $\beta(t)$. Physically, the TOMR accelerates for $\beta(t) < 0$ and the TOMR decelerates for $\beta(t) > 0$ in the translational motion. Since the boundary condition $v_t(t_f) = 0$ in *MTTP-C-SAS* creates a boundary condition $\beta(t_f) > 0$ for (21), the costate function is represented as $\beta(t) = \tilde{\alpha} e^{a(t - t_s)} + \alpha/a$, where $t_s (< t_f)$ is the switching time of the input vector and $\tilde{\alpha} = (\beta(t_f) - \alpha/a)\, e^{a(t_s - t_f)} (> 0)$. This finding means that the optimal input vector in *MTTP-C-SAS* has only one switching time.

C. Construction of an Optimal Input Vector

Based on the optimality condition, we discuss the generation of the optimal input vector in *MTTP-C-SAS*. Obviously, it is difficult to perform an analysis in the continuous time domain because of nonlinear coupling terms. Thus, we try to construct the optimal input vector in the discrete time domain with a time step size T. Using the information on the states $(\phi_k, \dot{\phi}_k, \psi_k, \dot{\psi}_k, s_k, v_k)$ at the *k*th time step$(t = kT)$ and a chosen input vector, we can determine the states $(\phi_{k+1}, \dot{\phi}_{k+1}, \psi_{k+1}, \dot{\psi}_{k+1}, s_{k+1}, v_{k+1})$ at the *(k+1)*th time step. For convenience, the simple notations for the representation of TOMR dynamics in this section are listed in Table II.

TABLE II
SIMPLE NOTATION FOR THE REPRESENTATION OF TOMR DYNAMICS IN THE DISCRETE TIME DOMAIN

Notation	Description
v_k	Translational velocity of TOMR at the k-th time step, i.e., $v_t(kT)$
c_k	Rotational input of TOMR at the k-th time step, i.e., $u_\phi(kT)$
Co_k	Normal input of TOMR at the k-th time step, i.e., $u_n(kT)$
γ_k	$\gamma_k = \phi_k - \psi_k$
C_i	$C_i = \cos(\gamma_k + 2(i-1)\pi/3)$, for i=1,2,3
S_i	$S_i = \sin(\gamma_k + 2(i-1)\pi/3)$, for i=1,2,3

The overall structure for the construction of the optimal input vector is represented with the following steps.

Step 1: Using the information on the previous states, calculate $u_\phi(kT)$ and $u_n(kT)$ at the *k*th time step.

Step 2: Using the optimality condition, determine an extreme input and the nonextreme inputs.

Step 3: From the optimal input vector, update the states at the *(k+1)*th time step.

Step 4: Repeat Steps 1, 2, and 3 until the TOMR reaches the final states.

In Step 1, we can choose the rotational input at the *k*th time step by the referenced heading information. Using the $\dot{\phi}$ dynamics and the relation $\dot{\phi} = g(s)v_t$

$$\dot{\phi}_k + T\left(-b\dot{\phi}_k + \frac{bh}{2l}c_k\right) = g(s_k)v_k. \tag{23}$$

From (23), c_k is represented as

$$c_k = \frac{2l}{bhT}\left(g(s_k)v_k - (1 - bT)\dot{\phi}_k\right). \tag{24}$$

In addition, from (16), the normal input at the *k*th time step is rewritten as

$$Co_k = -\frac{1}{ah}(\dot{\phi}_k - \kappa(s_k)v_k)v_k. \tag{25}$$

Then, we have only to choose the optimal input vector $\mathbf{u}^*$ with the optimality condition. We define the *Subproblem* for Step 2 as follows.

Subproblem: Find $\mathbf{u}^*$ subject to

$$\max(|u_1|, |u_2|, |u_3|) = 1 \tag{26}$$

$$Co_k = C_1 u_1 + C_2 u_2 + C_3 u_3 \tag{27}$$

$$c_k = u_1 + u_2 + u_3. \tag{28}$$

Since u_n and u_ϕ are considered to be constants for any instantaneous time, the translational input obtained by the optimality condition results in the minimum travel time. Hence, the solution of the *Subproblem* is the optimal input vector at the *k*th time step in *MTTP-C-SAS*. Here, (26) is the alternative expression of the optimality condition that is described in *Theorem 1* in Section III-B.

TABLE III
OPTIMAL INPUT VECTOR OF *MTTP-C-SAS*

Extreme input	Non-extreme inputs	Decomposed parts of optimal translational input
$u_3=1$	$u_1=\frac{2S_s}{3\sqrt{3}}\left(-\sqrt{3}S_1-c_kC_2+Co_k\right)$	$S_r=\frac{-c_k}{3}S_s$
	$u_2=\frac{2S_s}{3\sqrt{3}}\left(-\sqrt{3}S_2+c_kC_1-Co_k\right)$	$S_c=Co_k*\cot(\gamma_k+\frac{\pi}{3})$
$u_1=-1$	$u_2=\frac{2S_s}{3\sqrt{3}}\left(-\sqrt{3}S_2+c_kC_3-Co_k\right)$	$S_r=\frac{c_k}{3}S_s$
	$u_3=\frac{2S_s}{3\sqrt{3}}\left(-\sqrt{3}S_3-c_kC_2+Co_k\right)$	$S_c=Co_k*\cot(\gamma_k)$
$u_2=1$	$u_1=\frac{2S_s}{3\sqrt{3}}\left(-\sqrt{3}S_1+c_kC_3-Co_k\right)$	$S_r=\frac{-c_k}{3}S_s$
	$u_3=\frac{2S_s}{3\sqrt{3}}\left(-\sqrt{3}S_3-c_kC_1+Co_k\right)$	$S_c=Co_k*\cot(\gamma_k-\frac{\pi}{3})$
$u_3=-1$	$u_1=\frac{2S_s}{3\sqrt{3}}\left(-\sqrt{3}S_1+c_kC_2-Co_k\right)$	$S_r=\frac{c_k}{3}S_s$
	$u_2=\frac{2S_s}{3\sqrt{3}}\left(-\sqrt{3}S_2-c_kC_1+Co_k\right)$	$S_c=Co_k*\cot(\gamma_k-\frac{2\pi}{3})$
$u_1=1$	$u_2=\frac{2S_s}{3\sqrt{3}}\left(-\sqrt{3}S_2-c_kC_3+Co_k\right)$	$S_r=\frac{-c_k}{3}S_s$
	$u_3=\frac{2S_s}{3\sqrt{3}}\left(-\sqrt{3}S_3+c_kC_2-Co_k\right)$	$S_c=Co*\cot(\gamma_k+\pi)$
$u_2=-1$	$u_1=\frac{2S_s}{3\sqrt{3}}\left(-\sqrt{3}S_1-c_kC_3+Co_k\right)$	$S_r=\frac{c_k}{3}S_s$
	$u_3=\frac{2S_s}{3\sqrt{3}}\left(-\sqrt{3}S_3+c_kC_1-Co_k\right)$	$S_c=Co_k*\cot(\gamma_k+\frac{2\pi}{3})$

Note that S_s, S_r, S_c in the columns mean $S_s(\gamma_k)$, $S_r(\gamma_k)$, $S_c(\gamma_k)$, respectively, and that $S_s(\gamma_k)=\frac{3}{2}\left(\sin\left(\gamma_k-\left\lfloor\frac{3\gamma_k}{\pi}-1\right\rfloor\frac{\pi}{3}\right)\right)^{-1}$.

For example, when the extreme input component is $u_3 = 1$ (approximately, $0 < \phi_k - \psi_k < \pi/3$), we can determine the other two input components by (27), (28), and the trigonometric equalities

$$u_1 = \frac{2S_s(\gamma_k)}{3\sqrt{3}}\left(-\sqrt{3}S_1 - c_kC_2 + Co_k\right)$$
$$u_2 = \frac{2S_s(\gamma_k)}{3\sqrt{3}}\left(-\sqrt{3}S_2 + c_kC_1 - Co_k\right). \quad (29)$$

Here, $S_s(\bullet)$ is defined as the optimal translational input magnitude on the straight-line movement for the TOMR without changing the heading in [11].

Furthermore, from $\mathbf{u}^*$ and (14), we can decompose the optimal translational input u_t^* into three parts as

$$u_t^* = S_s(\gamma_k) + S_r(\gamma_k) + S_c(\gamma_k). \quad (30)$$

Physically, $S_r(\bullet)$ and $S_c(\bullet)$ represent the compensated inputs stemming from the constrained heading and curvature conditions in *MTTP-C-SAS*, respectively. Then, we summarize these decomposed parts as

$$S_r(\gamma_k) = \frac{-c_k}{3}S_s(\gamma_k), S_c(\gamma_k) = Co_k \times \cot(\gamma_k + \pi/3). \quad (31)$$

Repeating the calculation of nonextreme values for the remaining extreme input components besides $u_3 = 1$, we obtain Table III as a general solution of the *Subproblem* according to the extreme input.

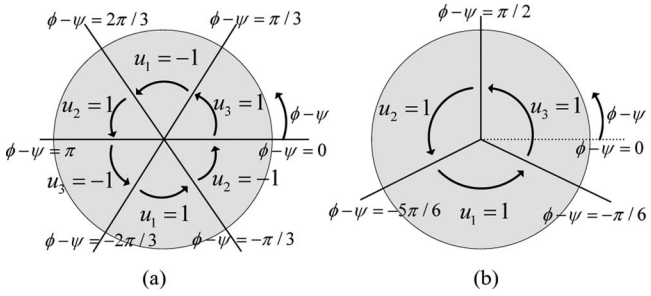

Fig. 6. Extreme input component according to the translational direction $\phi - \psi$ when $S_c = 0$ and $\dot{\phi} \geq \dot{\psi}$ (a) when $u_\phi = 0$ and (b) when $1 \leq u_\phi \leq 3$.

TABLE IV
PARAMETERS OF THE TOMR AND THE SAS PATH

TOMR Parameter	Value	SAS Parameter	Value
a	2.8368	B_s	0.5
b	6.1953	ψ_l	45°
h	0.6024	FS1	3 (m)
l	0.188 (m)	FS2	3 (m)

In Step 2, to apply Table III to construct the optimal voltage profile for the overall time, it is necessary to know which input in (26) is the extreme value. The extreme input component is determined by the forced direction of the TOMR, which depends on the angle difference between the TOMR heading and the path orientation, $\phi - \psi$. Considering the plane of $u_n = 0$ in Fig. 5 for various values of $\phi - \psi$, we can derive the relation between $\phi - \psi$ and the extreme component, as shown in Fig. 6.

Finally, in Step 3, the information on the states at the next time step is updated with the chosen optimal input vector. In Step 4, the boundary conditions of *MTTP-C-SAS* are checked to complete the calculation procedure of the optimal voltage profile. Concretely, whether Steps 1, 2, and 3 are repeated or not is determined by the translational velocity condition. The boundary condition of the final position is checked by the adjustment of the switching time of the optimal vector.

IV. SIMULATION

In this section, based on the result in Section III, we examine three examples with simple referenced heading profiles. The parameters of the TOMR and the SAS path used in the simulation are listed in Table IV, where the parameters of a, b, and h are calculated from [11, Table II]. Before the analysis of the simulation, we describe the form of the SAS path. FS1 and FS2 in Table IV refer to the lengths of the two straight lines that are connected to the clothoid arc in the SAS path. When we set B_s and ψ_l, as shown in Table IV, $B_{c,\max}$ is computed as 0.6267. With these parameters and various values of ψ_α, the SAS paths are shown in Fig. 7. The $'o'$, $'\Delta'$, $'\square'$, and $'\times'$ marks in Figs. 7, 9, and 11 represent the positions in the base coordinate frame for O_C, s_A, s_D, and s_F, respectively.

A. Straight-Line Path With Maintained Heading: $g(s) = \kappa(s) = 0$

Since $\kappa(s) = 0$ represents a straight line and $g(s) = 0$ represents a zero reference heading profile, we deal with the minimum-time trajectory following the straight-line path with no change of the TOMR heading in this section. Without loss of generality, we let the TOMR initially move in the positive x-direction, as noted in Section III-A.

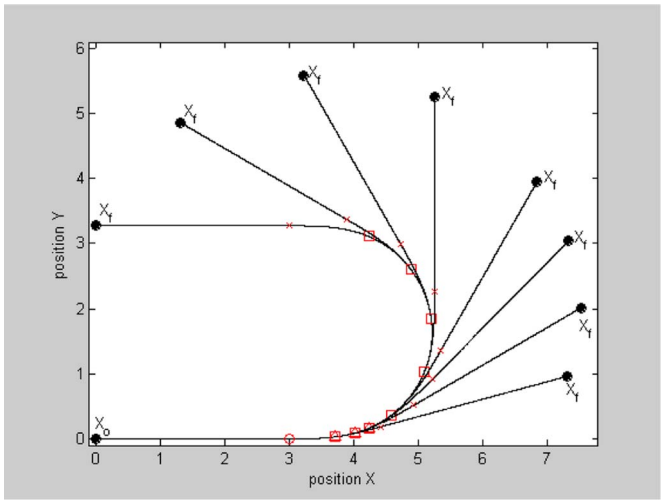

Fig. 7. SAS paths with various changes of path orientation of the clothoid. The SAS paths in the base coordinate frame for $\psi_\alpha = 15°, 30°, 45°, 60°, 90°, 120°, 150°$, and $180°$.

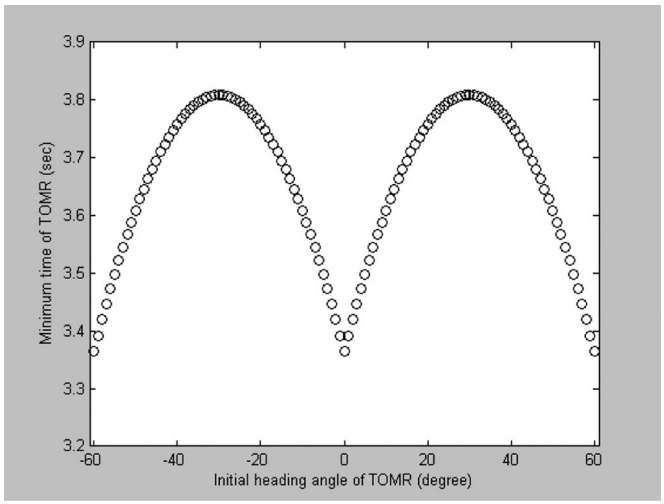

Fig. 8. Minimum travel time of the TOMR versus the initial heading angle at $g(s) = \kappa(s) = 0$.

Because $u_\phi = u_n = 0$, the values of c_k and Co_k in Table III are always zero. Thus, the magnitude of the optimal translational input depends only on $S_s(\phi_0)$. With the switching time of the optimal input vector t_s and the boundary conditions of *MTTP-C-SAS*, we can describe the linear velocity profile $\dot{x}^*(t)$ and the minimum time t_f as noted in [11]:

$$\dot{x}^*(t) = \begin{cases} S_s(\phi_0)h(1-e^{-at}), & \text{for } t \le t_s \\ S_s(\phi_0)h((1-e^{-at_s})e^{-a(t-t_s)} \\ \quad -(1-e^{-a(t-t_s)})), & \text{for } t > t_s \end{cases} \tag{32}$$

$$t_f = \frac{x_f}{S_s(\phi_0)h} + \frac{2}{a}\ln(1+\sqrt{G}) \tag{33}$$

where

$$G = 1 - e^{\frac{-a x_f}{S_s(\phi_0)h}}.$$

Fig. 8 shows the minimum-time pattern of the TOMR according to the initial heading angle when we set the final goal position $x_f = 3(m)$ for the simulation. Because of the symmetry of the result, the TOMR heading is restricted to the range $-60°$ to $+60°$. Although the TOMR moves in the same straight-line path, the TOMR moves faster with

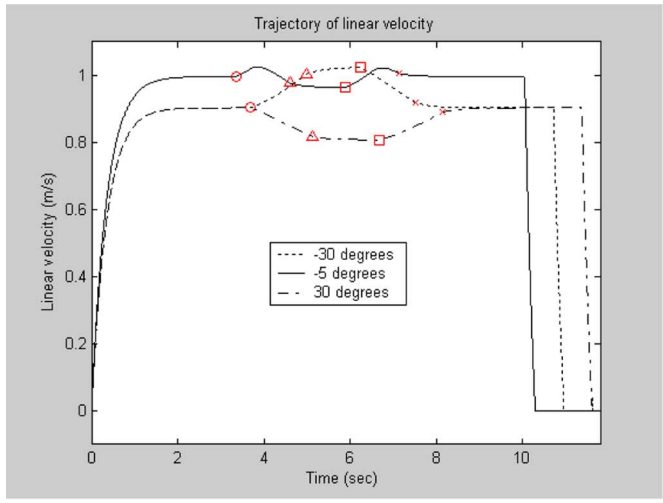

(a)

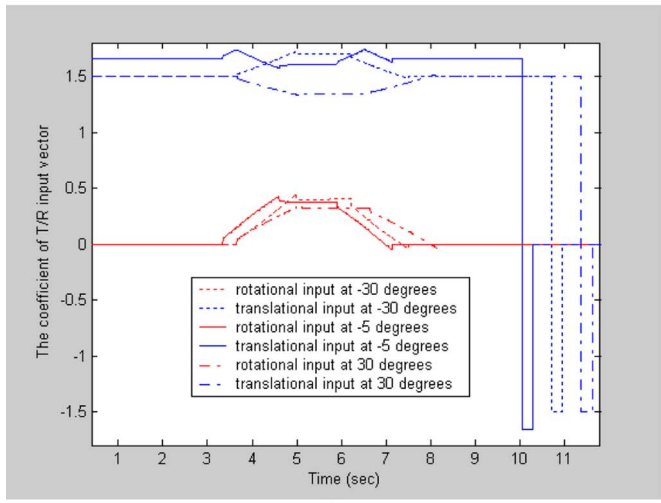

(b)

Fig. 9. Minimum-time trajectory of the TOMR with various initial heading angles when $\psi_\alpha = 90°$ and $g(s) = \kappa(s) \neq 0$. (a) Linear velocity profile at three sampled initial heading angles (solid line for $-5°$, dotted line for $-30°$, and dash dot line for $30°$). (b) Rotational/translational input profiles at three sampled initial heading angles. Blue indicates the translational input, and red indicates the rotational input. The angle information for line type is the same as in (a).

the optimal input vector of the *MTIP* shown in Fig. 5. This finding is because the minimum travel time of the TOMR depends only on $S_s(\phi_0)$, as shown in (33). The travel time of the TOMR with $\phi_0 = 30°$ is about 13.2% longer than the travel time with $\phi_0 = 60°$. In addition, the minimum travel time of the TOMR described in [20] is equal to the travel time of the TOMR with $\phi_0 = 30°$ in this paper, and it is the same for all translational directions. This is because the feasible input region in [20] is restricted to $\min_{\phi_0} S_s(\phi_0)$ for the heading independent control.

B. Straight–Arc–Straight Path With Maintained Difference Between Heading and Path Orientation: g(s) = κ(s) ≠ 0

To investigate how the rotational input affects u_t^*, we consider the reference heading profile with $g(s) = \kappa(s) \neq 0$ in this section. This $g(s)$ physically means that the difference between the TOMR heading and path orientation is maintained as a constant value

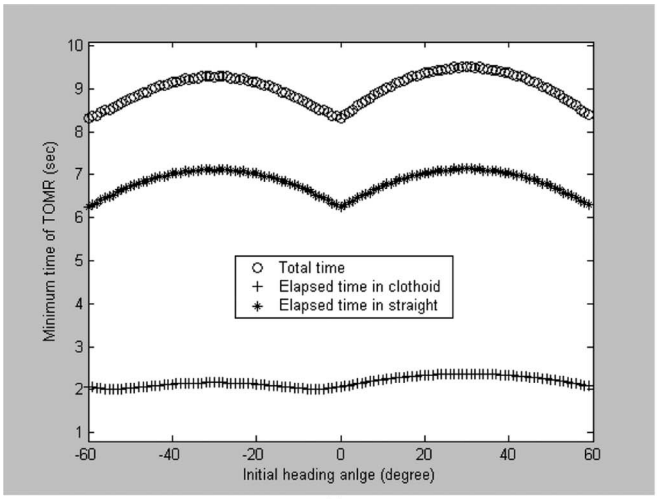

(a)

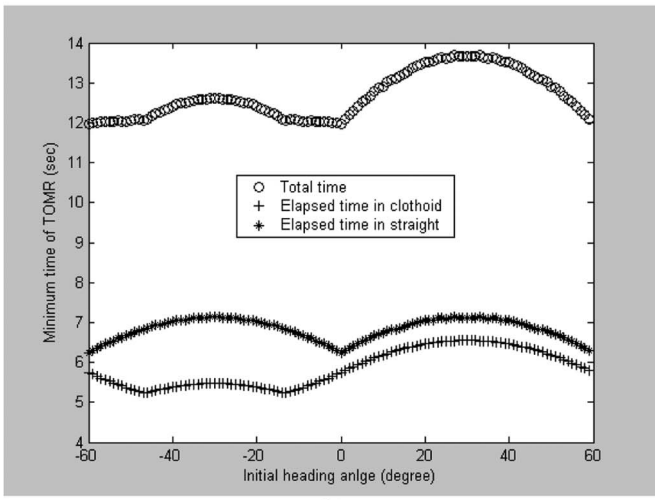

(b)

Fig. 10. Minimum travel time of the TOMR versus the initial heading angle at $g(s) = \kappa(s) \neq 0$. (a) $\psi_\alpha = 30°$. (b) $\psi_\alpha = 150°$.

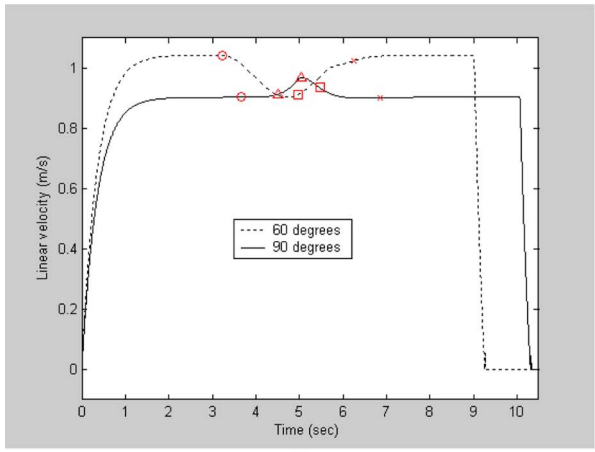

(a)

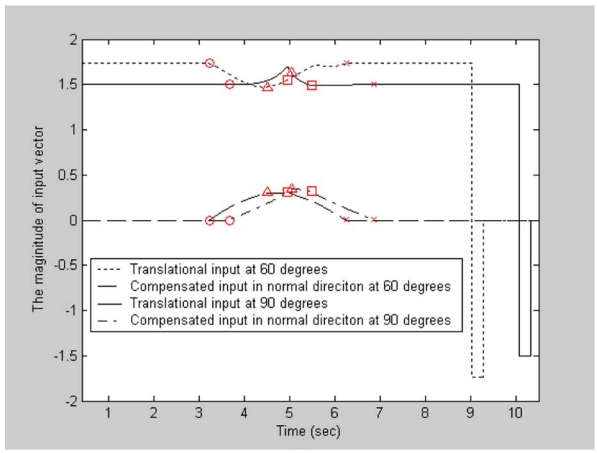

(b)

Fig. 11. Minimum-time trajectory of the TOMR when $\psi_\alpha = 60°$, $g(s) = 0$, and $\kappa(s) \neq 0$. (a) Linear velocity profiles at $\phi_0 = 60°$(dotted) and $\phi_0 = 90°$(solid). (b) Magnitude of translational input u_t (dotted line at $\phi_0 = 60°$ and solid line at $\phi_0 = 90°$) and compensated input $S_c(\bullet)$ (dash-dotted line at $\phi_0 = 60°$, dashed line at $\phi_0 = 90°$) of the optimal vector.

at any point in the SAS path. In other words, $\phi - \psi = \phi_0$ for any point in the SAS path. In this case, there is no compensation force in the normal direction to maintain the path, i.e., $u_n = 0$. Thus, the values of Co_k in Table III are always zero.

In this simulation, the minimum-time trajectories of the TOMR are made by the construction method for the optimal input vector proposed in Section III. Fig. 9 shows the linear velocity profile and the translational/rotational input profiles of the TOMR for the three sampled initial heading angles. The SAS path with $\psi_\alpha = 90°$ is used in Fig. 9.

We find that the linear velocity profile depends on the initial heading angle of the TOMR, as shown in Fig. 9. The reason for this result, as shown in Table III, is that the $S_s(\bullet)$ and $S_r(\bullet)$ parts of the translational input of the optimal vector depend on the initial heading angle ϕ_0. In other words, the minimum time of the TOMR depends on the initial heading. In particular, we note the importance of the sign of the compensated input $S_r(\bullet)$. For example, as shown in Fig. 6, the extreme input component is $u_3 = 1$ for $\phi_0 = 30°$. Then, from Table III, $S_r(\bullet)$ decreases the magnitude of the optimal translational input. Conversely, for a negative initial heading angle, the extreme input component is $u_2 = -1$, and $S_r(\bullet)$ increases the magnitude of the optimal translational input. This phenomenon is directly observed in Fig. 9(a).

The second simulation is performed to verify the minimum-time pattern according to the initial heading angles. Because of the symmetric structure of the TOMR, we perform the simulation for initial heading angles in the range $-60° \leq \phi_0 \leq 60°$ with $1°$ increments. As shown in Fig. 10, the minimum-time solution of *MTTP-C-SAS* varies with the initial heading angles. The elapsed time on the straight line has minima at $\phi_0 = -60°, 0°, 60°$. However, the elapsed time on the clothoid arc has minima at near zero and $-60°$ [$\phi_0 \cong -6°, -54°$ in Fig. 10(a) and $\phi_0 \cong -14°, -46°$ in Fig. 10(b)].

Thus, the TOMR can move faster along an SAS path when the initial heading angle is between the minimum for the clothoid arc and the minimum for the straight line, as shown by the $'o'$ marks in Fig. 10. These results explain why the minimum travel time of the TOMR in *MTTP-C-SAS depends on the initial heading angle* even though the TOMR moves along the same SAS path with the same reference heading profile.

C. Straight–Arc–Straight Path With Maintained Heading: $g(s) = 0$ and $\kappa(s) \neq 0$

In this section, to investigate how coupling terms in the TOMR dynamics affect u_t^*, we consider the reference heading profile with $g(s) = 0$. This $g(s)$ physically means that the TOMR moves along the

SAS path while the heading of the TOMR is maintained at the same value as the initial heading angle. In other words, $\phi \equiv \phi_0 (= \phi_f)$ for any point on the SAS path. Thus, there is no rotational input while the TOMR moves along the SAS path, i.e., $u_\phi \equiv 0$, and the values of c_k and $S_r(\bullet)$ in Table III are always zero.

In this simulation, the SAS path with $\psi_\alpha = 60^\circ$ is given for the curved path. Fig. 11 shows the linear velocity profiles and the translational/compensated input profiles of the TOMR for two initial heading angles ($\phi_0 = 60^\circ, 90^\circ$). From $u_\phi = 0$, we obtain $\dot{\phi} = 0$ and $u_n = (ah)^{-1}\dot{\psi}v_t$. Thus, we can represent the optimal translational input of the TOMR at any point on the SAS path as $u_t^* = S_s(\phi - \psi) + S_c(\phi - \psi)$. As shown in Fig. 11(a), the linear velocity along the clothoid is different from that along the straight line. This difference occurs because the $S_s(\bullet)$ depends on $\phi - \psi (= \phi_0 - \psi)$. Therefore, although the TOMR moves along the same SAS path with the same reference profile, the velocity pattern changes, depending on the selection of ϕ_0. Furthermore, Fig. 11(b) shows that the $S_c(\bullet)$ part of the optimal translational input should not be neglected in the clothoid arc.

V. Conclusion

A. Advantage Over Any Other Approach

This paper focuses on the time-optimal trajectory for a TOMR with a reference heading profile following an SAS path. Considering TOMR dynamics, we find that the optimality condition for the motor control input vector is at least *one-extreme*. We also propose a general method for the construction of the optimal input vector. Additionally, we find that the minimum travel time of the TOMR depends on the initial heading, even when the TOMR moves along the same path.

Rather than any other near-time-optimal trajectories based on the restricted feasible input region, we consider the full feasible input region based on TOMR dynamics for time optimality. Furthermore, the proposed method for the construction of the optimal input vector is applicable to arbitrarily smooth paths parameterized by path lengths. In other words, our construction method is not restricted to the form of a planar path and a reference heading profile.

B. Discussion

In this paper, we do not argue that TOMRs can move faster on the specific SAS paths with specific reference heading profiles. We also do not yet consider the time-optimal trajectory of TOMRs along SAS paths with heading freedom, that is, without a reference heading profile. In that case, we can expect that the optimal vector will be at least *two-extreme*. The related work on a straight-line path is shown in [23].

In this paper, we deal with the control input profile in the open loop for the time-optimal trajectory. For implementation in real applications, if we can convert the time-optimal solution to feedback form, i.e., the control input vector as a function of state, we can apply the time-optimal feedback controller. In addition, while our analysis is based on TOMR dynamics, we have not yet dealt with another technical topic, e.g., the sensitivity of the robot parameters. These topics will be studied in the near future.

References

[1] F. G. Pin and S. M. Killough, "A new family of omnidirectional and holonomic wheeled platform for mobile robots," *IEEE Trans. Robot. Autom.*, vol. 10, no. 4, pp. 480–489, Aug. 1994.

[2] X. Gao, Y. Wang, D. Zhou, and K. Kikuchi, "Floor-cleaning robot using omni-directional wheels," *Int. J. Ind. Robot.*, vol. 36, no. 2, pp. 157–164, 2009.

[3] S. Wang, K. Kawata, Y. Inoue, K. Ishida, and T. Kimura, "Omni-directional mobile walker for rehabilitation of waking which can prevent tipping over," in *Proc. Jpn. Soc. Mech. Eng. Symp. Welfare Eng.*, Tokyo, Japan, 2003, pp. 145–146.

[4] A. Koestler and T. Braunl, "Mobile robot simulation with realistic error models," in *Proc. Int. Conf. Auton. Robots Agents*, Palmerston, New Zealand, Dec. 2004, pp. 46–51.

[5] M. Riedmiller, T. Gabel, R. Hafner, and S. Lange, "Reinforcement learning for robot soccer," *Auton. Robots*, vol. 27, no. 1, pp. 55–73, 2009.

[6] K. Terashima, T. Miyoshi, J. Urbano, and H. Kitagawa, "Frequency shape control of omni-directional wheelchair to increase user's comfort," in *Proc. IEEE Int. Conf. Robot. Autom.*, New Orleans, LA, 2004, pp. 3119–3124.

[7] H. C. Huang and C. C. Tsai, "Adaptive robust control of an omnidirectional mobile platform for autonomous service robots in polar coordinates," *J. Intell. Robot. Syst.*, vol. 51, no. 4, pp. 439–460, 2008.

[8] O. Purwin and R. D'Andrea, "Trajectory generation and control for four wheeled omnidirectional vehicles," *Robot. Auton. Syst.*, vol. 54, no. 1, pp. 13–22, 2006.

[9] R. Rojas and A. G. Foerster, "Holonomic control of a robot with an omnidirectional drive," *Kuenstliche Intelligenz*, vol. 20, no. 2, pp. 12–17, 2006.

[10] K. Watanabe, Y. Shiraishi, S. G. Tzafestas, J. Tang, and T. Fukuda, "Feedback control of an omnidirectional autonomous platform for mobile service," *J. Intell. Robot. Syst.*, vol. 22, no. 3, pp. 315–330, 1998.

[11] K. B. Kim and B. K. Kim, "Minimum-time straight-line trajectory for three-wheeled omni-directional mobile robots with voltage constraints," in *Proc. 39th Int. Symp. Robot.*, Seoul, Korea, 2008, pp. 755–760.

[12] J. S. Choi and B. K. Kim, "Near-time-optimal trajectory planning for wheeled mobile robots with translational and rotational sections," *IEEE Trans. Robot. Autom.*, vol. 17, no. 1, pp. 85–90, Feb. 2001.

[13] A. J. Hejase, "Optimal motion synthesis of a mobile robot," in *Proc. IEEE Int. Workshop Intell. Motion Control*, Istanbul, Turkey, 1990, vol. 2, pp. 897–901.

[14] V. Munoz, A. Ollero, M. Prado, and A. Simon, "Mobile robot trajectory planning with dynamics and kinematics constraints," in *Proc. IEEE Int. Conf. Robot. Autom.*, San Diego, CA, 1994, vol. 4, pp. 2802–2807.

[15] M. Renaud and J. Y. Fourquet, "Minimum time motion of a mobile robot with two independent, acceleration-driven wheels," in *Proc. IEEE Int. Conf. Robot. Autom.*, Albuquerque, NM, 1997, vol. 3, pp. 2608–2613.

[16] N. Faiz and S. K. Agrawal, "Trajectory planning of robots with dynamics and inequality," in *Proc. IEEE Int. Conf. Robot. Autom.*, San Francisco, CA, 2000, vol. 4, pp. 3976–3982.

[17] D. J. Balkcom and M. T. Mason, "Time optimal trajectory for bounded velocity differential drive robot," in *Proc. IEEE Int. Conf. Robot. Autom.*, San Francisco, CA, 2000, vol. 3, pp. 2499–2504.

[18] C. G. L. Bianco, A. Piazzi, and M. Romano, "Smooth motion generation for unicycle mobile robots via dynamic path inversion," *IEEE Trans. Robot.*, vol. 20, no. 5, pp. 884–891, Oct. 2004.

[19] H. Chitsaz, S. M. Lavalle, D. J. Balkcom, and M. T. Mason, "Minimum wheel-rotation paths for differential-drive mobile robots," *Int. J. Robot. Res.*, vol. 28, no. 1, pp. 66–80, 2009.

[20] T. Kalmar-Nagy, R. D'Andrea, and P. Ganguly, "Near-optimal dynamic trajectory generation and control of an omnidirectional vehicle," *Robot. Auton. Syst.*, vol. 46, no. 1, pp. 47–64, 2004.

[21] Y. Y. Fu, C. N. Ko, T. L. Lee, and C. J. Wu, "A nonlinear programming method for time-optimal control of an omni-directional mobile robot," *J. Vib. Control*, vol. 14, no. 11, pp. 1729–1747, 2008.

[22] D. J. Balkcom, P. A. Kavathekar, and M. T. Mason, "Time-optimal trajectories for an omni-directional vehicle," *Int. J. Robot. Res.*, vol. 25, no. 10, pp. 985–999, 2006.

[23] K. B. Kim and B. K. Kim, "A new approach to time-optimal trajectory for omni-directional mobile robots with multi-objective costs," in *Proc. IEEE Int. Conf. Robot. Autom.*, Anchorage, AK, 2010, pp. 1991–1996.